Chemical Science

ROYAL SOCIETY OF CHEMISTRY

EDGE ARTICLE

View Article Online
View Journal | View Issue

Check for updates

Cite this: *Chem. Sci.*, 2025, **16**, 19215

All publication charges for this article have been paid for by the Royal Society of Chemistry

Dual-site recognition leads to a ratiometric fluorescent probe for norepinephrine: quantitative detection and visualization for in-depth understanding of hypertension

Fengzhi Wang,[a] Jiawen Wang,[a] Weiping Zhu,[a] Yangyang Yang,[a] Honglin Li,*[ad] Tony D. James,*[bc] Yufang Xu*[a] and Xuhong Qian[ad]

Hypertension is closely associated with the activation of sympathetic nervous system (SNS). Norepinephrine (NE) belongs to the catecholamine family and is the primary neurotransmitter of SNS. Plasma and tissue NE levels serve as biomarkers of sympathetic overdrive in hypertension, providing measurable indicators to guide therapeutic approaches. However, there are only a few reliable tools to simultaneously quantify plasma NE and visualize tissue NE for comprehensive SNS assessment in hypertension. Herein, to selectively recognize the unique L-hydroxyethylamine and catechol moieties of NE, we designed and synthesized a dual-site fluorescent probe that can specifically bind to these two characteristic groups. The recognition process generates a macrocyclic-ring enhanced by silver bridging, accompanied by a ratiometric fluorescence change. The probe enables quantitative NE detection in both plasma and urine, as well as NE visualization in heart, kidney and adrenal gland tissues. Notably, our results demonstrated that spontaneously hypertensive rats (SHR) have higher circulating and tissue NE levels, indicating SNS overactivation. These findings provide a powerful molecular tool for the assessment of SNS activity and offer an in-depth understanding of hypertension.

Received 6th August 2025
Accepted 12th September 2025

DOI: 10.1039/d5sc05925a

rsc.li/chemical-science

Open Access Article. Published on 15 September 2025. Downloaded on 2/10/2026 10:16:37 AM. This article is licensed under a Creative Commons Attribution-NonCommercial 3.0 Unported Licence.

Introduction

Blood pressure has long been regarded as a typical cardiovascular function, which is closely associated to sympathetic nervous system (SNS) activity.[1,2] Norepinephrine (NE), a member of the catecholamine family (including dopamine, norepinephrine and epinephrine) (Fig. 1a), is the primary neurotransmitter of SNS.[3–8] Upon sympathetic activation, postganglionic neurons release NE, which acts on the target organs to modulate cardiovascular function and contribute to the blood pressure through adrenergic receptor signaling.[9–15] The release of NE is directly correlated with neural activity, making NE a reliable indicator for evaluating SNS activity.[16,17] Plasma and tissue NE levels serve as biomarkers of sympathetic overactivation in hypertension, and their quantification can guide the development of therapeutic strategies.[18–20] However, the low amount, easy oxidation and multiple interferences for NE make the accurate detection challenging. To date, high performance liquid chromatography (HPLC),[21,22] enzyme-linked immunosorbent assays (ELISA) and electrochemical methods[23–26] have been used for the quantification of NE, but they are limited by sensitivity and poor spatial resolution. In contrast, a promising alternative is fluorescence-based analysis which provides high sensitivity and superior spatiotemporal resolution with cellular precision. However, to our knowledge, there are only a few molecular tools capable of simultaneously quantifying plasma NE and visualizing tissue NE for comprehensive assessment of SNS in hypertension.

Currently available NE fluorescent probes are mostly based on the cascade nucleophilic reactions of the hydroxyethylamine moiety in NE.[27–30] Yin's group have used carbonate as the reactive site to recognize hydroxyethylamine which exhibited "off–on" fluorescence response with a detection limit of 64.3 μM.[29,30] Tian's group reported a fluorescent probe that can quickly respond to NE with "on–off" fluorescence and proposed an accelerated mechanism using folding and water-bridging.[27,28,31] Glass's group used an aldehyde group to recognize the hydroxyethylamine while using a boronic acid to bind with catechol to increase the binding efficiency (Fig. 1b).[32–36] These reported NE probes are based on using a single recognition site or a single-channel fluorescence change, from which

[a]*Shanghai Key Laboratory of Chemical Biology, School of Pharmacy, East China University of Science and Technology, Shanghai, 200237, China. E-mail: yfxu@ecust.edu.cn; hlli@hsc.ecnu.edu.cn*

[b]*Department of Chemistry, University of Bath, BA2 7AY Bath, UK. E-mail: T.D.James@bath.ac.uk*

[c]*School of Chemistry and Chemical Engineering, Henan Normal University, Xinxiang, 453007, China*

[d]*Innovation Center for Artificial Intelligence and Drug Discovery, East China Normal University, Shanghai, 200241, China*

© 2025 The Author(s). Published by the Royal Society of Chemistry

Open Access Article. Published on 15 September 2025. Downloaded on 2/10/2026 10:16:37 AM.
This article is licensed under a Creative Commons Attribution-NonCommercial 3.0 Unported Licence.

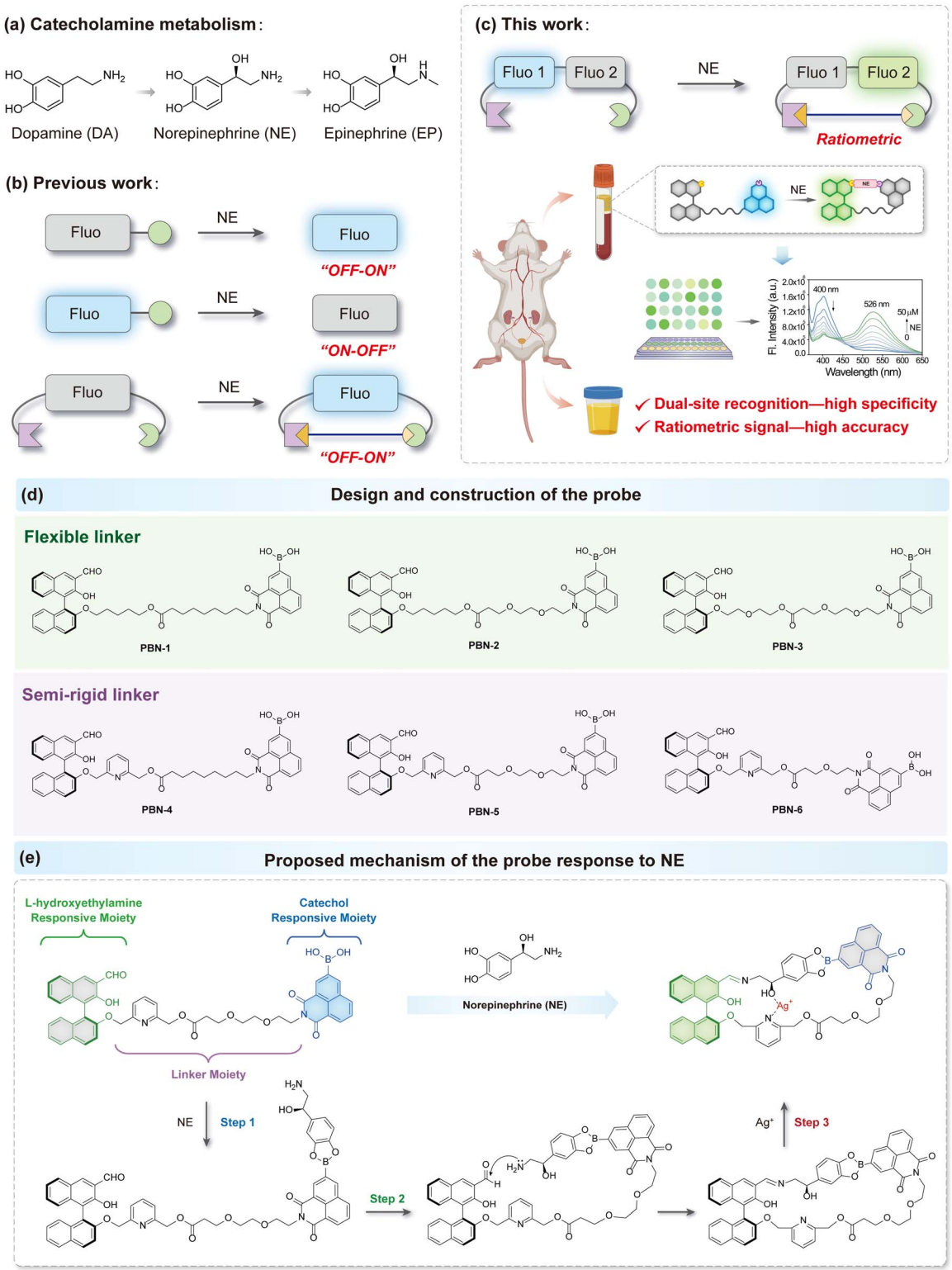

Fig. 1 General design of the fluorescent probe for specific quantification of NE. (a) Structures and metabolism of catecholamines. (b) Schematic illustration of the reported NE fluorescent probes based on single-site or dual-site recognition strategies. (c) Schematic illustration of the dual-site ratiometric NE fluorescent probe based on the cyclization recognition strategy in this work, as well as the application for quantifying plasma and urinary NE of hypertensive rats. (d) Design and construction of the PBN probes. (e) Proposed mechanism for the response of probe PBN-5 towards NE.

it is easy to be interfered with by amino acids (10–500 μM) making it hard to achieve specific and quantitative detection due to a lack of self-calibration.[37] As such, it is of significant importance to develop highly-selective and quantifiable fluorescent probes for the precise and specific high-throughput detection of NE.

© 2025 The Author(s). Published by the Royal Society of Chemistry

Open Access Article. Published on 15 September 2025. Downloaded on 2/10/2026 10:16:37 AM. This article is licensed under a Creative Commons Attribution-NonCommercial 3.0 Unported Licence.

Ratiometric signal measurements can reduce the interference associated with probe concentration, excitation intensity and the environment through the calibration of two emission channels, thereby providing an ideal method for quantitative analysis.[38,39] In this respect, a probe for the specific and quantitative detection of NE should meet at least two prerequisites: (1) it should simultaneously recognize the two characteristic groups of NE: hydroxyethylamine and catechol, respectively. (2) The recognition preferably produces a ratiometric fluorescence signal which exhibits no crosstalk. The cyclization recognition strategy has been used for fluorescence recognition of amino acids, exhibiting advantages of high specificity and affinity.[40,41] The recognition process increases the structural rigidity of the macrocycle and suppresses the excited state isomerization, which facilitates fluorescence turn-on.[42] Significantly, the cavities of macrocycles can also provide binding sites for ions and hydrogen bonds to improve the detection performance of such probes.[43]

Here, we report a dual-site fluorescent probe, **PBN-5**, combining a cyclization recognition strategy with ratiometric signals to achieve selective quantification of NE (Fig. 1c). An aldehyde and boronic acid group were used as the two sites to bind with NE and form a macrocyclic-ring, a ratiometric signal was obtained to distinguish NE from other biological nucleophiles. Significantly, the addition of silver ions accelerated the recognition and amplified the signal by chelating with the as-formed macrocyclic-ring using silver bridging. Compared with the previously reported "off–on" probes, the ratiometric probe **PBN-5** exhibits excellent anti-interference capability, thus providing higher accuracy for quantitative analysis. Notably, plasma NE and urinary NE of spontaneously hypertensive rats (SHR) and normotensive Wistar-Kyoto (WKY) rats were compared using our probe. Additionally, we investigated the NE levels in sympathetic nerve-rich cardiac, renal and adrenal gland tissues of both SHR and WKY rats to assess sympathetic-adrenal activity. This reliable probe serves as a valuable tool for the comprehensive study of the relationship between NE and SNS-associated diseases such as hypertension.

Results and discussion

Design and synthesis of PBN probes

To achieve the quantification of NE, the fluorescent probe needs to have both specificity and accuracy. For high specificity, a dual-site recognition strategy based on the unique structure of NE was used. While to achieve high accuracy, a ratiometric signal response was used for quantitative analysis, which is less influenced by environmental factors.

We first analyzed the chemical structure of NE and identified two active reactive groups: β-hydroxyethylamine and catechol. β-Hydroxyethylamine exhibits nucleophilic properties, as it can undergo a nucleophilic reaction with aldehyde groups. While boronic acid is a well-known functional group that can selectively recognize 1,2-diols or 1,3-diols to form five- or six-membered cyclic esters. Thus, we used a boronic acid group to bind with the two adjacent hydroxyl groups of catechol. Meanwhile, amino acids or other biological nucleophiles, as well as other catecholamine homologs, do not possess both groups simultaneously, allowing for the selective recognition to NE.

The two fluorophores need to be excited at the same wavelength and generate a fluorescence increase and decrease independently with low levels of crosstalk after recognition. The hydroxyethylamine of NE is in a L-configuration, which is also one of the structural characteristics. While, 1,1′-bi-2-naphthol (BINOL) has been widely investigated for the enantioselective recognition of amino acids.[44–46] Inspired by chiral recognition, we chose (*S*)-BINOL as a fluorophore containing an aldehyde as the hydroxyethylamine reaction site, which may exhibit significant fluorescence enhancement after binding and chiral matching with L-hydroxyethylamine. While naphthalimide was chosen as the other fluorophore due to the excellent matching of the excitation wavelength with that of (*S*)-BINOL, and the boronic acid group was chosen as the catechol reaction site to generate fluorescence quenching as induced by the electron-rich catechol of NE (Fig. 1c and e). As such, when the probe reacts with NE, the ratiometric fluorescence signal between the two fluorophores enables the quantification of NE.

The two recognition sites were connected by a linker, and the linker was varied to determine the most sensitive recognition system. Thus, we designed six compounds belonging to two series: **PBN-1–3** contained flexible linkers; **PBN-4–6** contained semi-rigid linkers with pyridine group to provide potential hydrogen bond interaction sites (Fig. 1d). The synthesis and characterization of the probes are given in the SI.

Spectral response and selectivity of the probe PBN-5

The response of the six probes designed above for NE was determined in PBS buffer (10 mM, pH = 7.4, 10% DMSO). To investigate the linker effect on the probes, we focused on the reaction kinetics. As shown in Fig. S1, the emission intensity at 400 nm decreased immediately, accompanied by a slower increase at 530 nm after mixing with NE within 50 min.

It is worth noting that the fluorescence of **PBN-1–PBN-4** at 400 nm was suppressed, presumably due to the freedom of two fluorophores when using flexible linkers (Fig. S1a, c, e and g). The fluorescence at 526 nm occurred without the analytes in both **PBN-1**, **PBN-2**, **PBN-4** and **PBN-5** (Fig. S1a, c, g and i). It may be due to intramolecular hydrogen bonding interactions between the hydroxyl group of binaphthyl and boronic acid, which leads to the twisting of (*S*)-BINOL and the appearance of fluorescence. Thus, the results above indicated that semi-rigid linkers are more favorable for constructing dual-site probes when compared to fully flexible linkers, and **PBN-5** was superior to other compounds. We speculated that the appropriate length and freedom of the linker made it easier for **PBN-5** to combine with NE to form a cyclic compound. Thus, **PBN-5** was subsequently evaluated using additional recognition and mechanism studies.

The fluorescence response of **PBN-5** towards NE was evaluated in PBS buffer. A new emission peak at 526 nm appeared and gradually increased, accompanied by a fluorescence decrease at 400 nm with the addition of NE (Fig. 2a and b). The

Open Access Article. Published on 15 September 2025. Downloaded on 2/10/2026 10:16:37 AM.
This article is licensed under a Creative Commons Attribution-NonCommercial 3.0 Unported Licence.

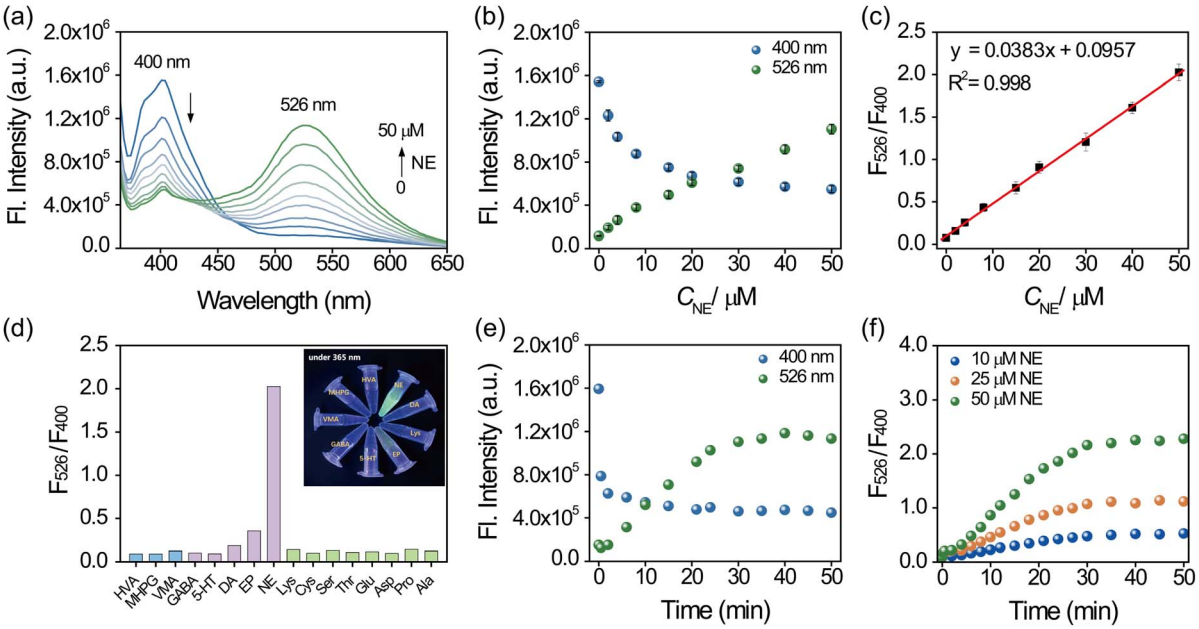

Fig. 2 The photophysical properties and *in vitro* response to NE of probe **PBN-5**. (a) Fluorescence spectra of **PBN-5** (10 μM) upon the addition of NE (0–50 μM) in PBS buffer (10 mM, pH = 7.4, 10% DMSO), excited at 350 nm. (b) Fluorescence intensity of **PBN-5** at 400 nm and 526 nm upon the addition of NE in PBS buffer. Data are presented as mean ± S.D. Error bars: S.D., $n = 5$ independent experiments. (c) Plot and linear fitting of the fluorescence variation (F_{526}/F_{400}) as a function of the concentrations of NE (0–50 μM). Data are presented as mean ± S.D. Error bars: S.D., $n = 5$ independent experiments. (d) Selectivity of **PBN-5** towards NE and other neurotransmitters (DA, EP, 5-HT, GABA), catecholamine metabolites (HVA, MHPG, VMA) and amino acids (Lys, Cys, Ser, Thr, Glu, Asp, Pro, Ala) (50 μM for each). Insert: color photograph under 365 nm excitation in the dark. (e) Time dependence of **PBN-5** upon the addition of 50 μM NE for 0–50 min at 400 nm and 526 nm, respectively. (f) Time dependence of **PBN-5** upon 10 μM, 25 μM, 50 μM NE for 0–50 min at F_{526}/F_{400}.

fluorescence intensity ratio of the dual channels (F_{526}/F_{400}) *versus* the concentration of NE was plotted in Fig. 2c, and exhibited good linearity within a concentration range of 0–50 μM NE. Given that complex biological environments might interfere with detection, the selectivity of **PBN-5** towards NE was evaluated against other catecholamine homologues (DA, EP), catecholamine metabolites (HVA: the metabolite of DA, MHPG: the metabolite of NE, VMA: the metabolite of EP), neurotransmitters (5-HT, GABA), and amino acids in both PBS buffer and plasma. The results indicated that the fluorescence at 400 nm decreased with catecholamine homologues (DA, EP), while the signal at 526 nm was less affected by these analytes (Fig. S4). The ratio of the dual channels (F_{526}/F_{400}) exhibited high selectivity for NE in both PBS buffer and plasma (Fig. 2d and S5). The reaction was completed within 30 min according to the reaction kinetic experiments (Fig. 2e and f). These results confirmed that probe **PBN-5** can effectively recognize NE with high sensitivity and selectivity.

Response mechanism of the probe PBN-5 to NE

To further elucidate the recognition mechanism, ^{1}H NMR and MALDI-TOF MS for the reaction between **PBN-5** and NE were conducted. As shown in Fig. 3a, **PBN-5** exhibited a singlet at δ 10.33 ppm for the aldehyde proton. The aldehyde group formed an intramolecular hydrogen bond with *o*-hydroxyl group, which led to a highly downfield-shifted hydroxyl signal at δ 10.22 ppm. The addition of NE led to the disappearance of the aldehyde signal, and a new peak gradually appeared at δ 8.76 ppm. This new peak can be assigned to an imine proton formed from the condensation of the aldehyde group of **PBN-5** and the amino group of NE. The intramolecular hydrogen bond between the aldehyde and hydroxyl group was also disrupted, resulting in a chemical shift of the hydroxyl signal to a higher field at δ 9.21 ppm.

Meanwhile, the addition of NE led to the disappearance of the boronic acid protons (δ 8.58 ppm), accompanied by a chemical shift of the *ortho* aromatic proton signals to a higher field, indicating the condensation of the boronic acid of **PBN-5** and the catechol of NE. Three new singlets at δ 6.38–6.48 ppm were observed in both experiments that belong to the benzene ring of NE. The mass spectra (MALDI-TOF) of the reaction mixture revealed the coexistence of multiple binding products (boronic acid binding complex **PBN-NE-1**, aldehyde binding complex **PBN-NE-2**, and dual-site macrocyclic binding complex **PBN-NE-cyclic**) in the reaction system (Fig. 3b). Among them, the signal observed at m/z = 934.3 exhibited the highest intensity, which could be attributed to the product **PBN-NE-cyclic** (calcd for [**PBN-NE-cyclic** + H]$^+$, 934.3). These results confirmed that **PBN-5** reacted with NE and formed a cyclic compound as expected.

In order to rationalize the ratiometric fluorescence singal, two control compounds (**(S)-P1** and **N1**) containing the two recognition sites of **PBN-5**, respectively, were designed and synthesized (Fig. 3c). As we expected, both **(S)-P1** and **N1** exhibited a significant response with NE. An obvious fluorescence increase at 526 nm was observed after mixing probe **(S)-P1**

© 2025 The Author(s). Published by the Royal Society of Chemistry

Open Access Article. Published on 15 September 2025. Downloaded on 2/10/2026 10:16:37 AM. This article is licensed under a Creative Commons Attribution-NonCommercial 3.0 Unported Licence.

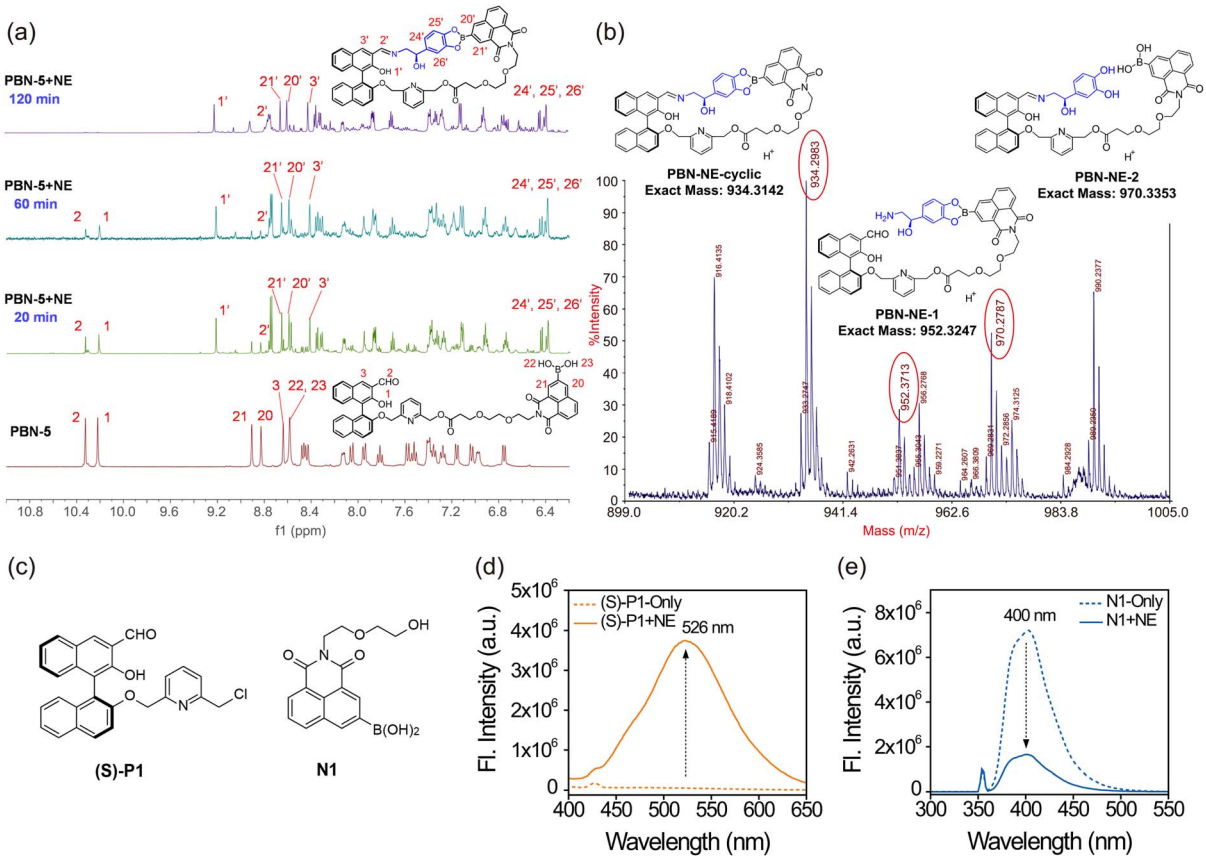

Fig. 3 Response mechanism characterization of probe **PBN-5** towards NE. (a) ^{1}H NMR spectra of the reaction mixture of **PBN-5** with NE at various reaction times in DMSO-d_6. (b) MALDI-TOF MS of the reaction mixture of **PBN-5** with NE. (c) Chemical structures of control molecules (***S*)-P1** and **N1**. (d) Fluorescence spectra of (***S*)-P1** (10 μM) upon addition of 1 mM NE in PBS buffer (10 mM, pH = 7.4, 10% DMSO), excited at 350 nm. (e) Fluorescence spectra of **N1** (10 μM) upon addition of 1 mM NE in PBS buffer (10 mM, pH = 7.4, 10% DMSO), excited at 350 nm.

with NE (Fig. 3d), while probe **N1**, with a pK_a of 8.76 (Fig. S6), exhibited fluorescence quenching at 400 nm upon the incubation with NE (Fig. 3e), suggesting that the boronic acid group binds catechol in its neutral form rather than the hydroxylated form. More importantly, the binding affinity of **N1** (with a binding constant $K_a = 9634\ M^{-1}$) for NE is significantly higher than that of **(S)-P1** ($K_a = 1927\ M^{-1}$), which indicated the difference in NE-binding affinity between the two reactive sites of **PBN-5** (Fig. S7). These results could account for the coexistence of multiple binding products in the MALDI-TOF MS (Fig. 3b), and it could contribute to the absence of an isosbestic point in the fluorescence titration curves (Fig. 2a). We also studied the fluorescence response of two enantiomers **(*S*)-P1** and **(*R*)-P1** towards NE under the same conditions, and **(*S*)-P1** generated a higher fluorescence enhancement at 526 nm than **(*R*)-P1** (Fig. S8). These results indicated that the boronic acid group of **PBN-5** combined with catechol causing the fluorescence quenching of naphthalimide due to the electron-rich catechol. Meanwhile, the aldehyde group of **PBN-5** combined with the amino group of NE to generate an imine, which enhanced the fluorescence at 526 nm by matching the chiral configuration to the twist of the binaphthyl plane. A ratiometric signal was observed after the recognition process which is consistent with our design presented in Fig. 1.

Effects of metal cations on the recognition of NE

Time-dependent experiments indicated that the fluorescence increase at 526 nm caused by the combination of aldehyde and the NE amino group is the rate-limiting process. As such, we wondered whether there was any way to accelerate the reaction in order to improve the detection efficiency. Metal cations, act as Lewis acids and can accept electron pairs. Therefore, they can form coordinative bonds with nucleophiles, such as amino groups, to enhance the nucleophilicity and accelerate imine formation with aldehydes. The addition of metal cations to BINOL-based chiral probe system is anticipated to enhance the fluorescence response through coordination with N/O atoms,[47,48] thereby promoting the recognition process.

The fluorescence intensity of **PBN-5** remained unchanged after titrating with 11 metal cations (Fig. S9). Subsequently, the fluorescence response of **PBN-5** towards NE was determined in the presence of the 11 metal cations in PBS buffer. The results indicated that certain metal cations (Na^+, Ca^{2+}, Fe^{2+}, Mg^{2+}, Fe^{3+}) shortened the equilibrium time to approximately 20 min without enhancing the fluorescence signal (Fig. S10). Notably, after the addition of Ag^+, the equilibration time was significantly reduced to 15 min, while the signal of the probe at F_{526}/F_{400} was also amplified by 3.85-fold (Fig. 4a and b). The MALDI-

Open Access Article. Published on 15 September 2025. Downloaded on 2/10/2026 10:16:37 AM. This article is licensed under a Creative Commons Attribution-NonCommercial 3.0 Unported Licence.

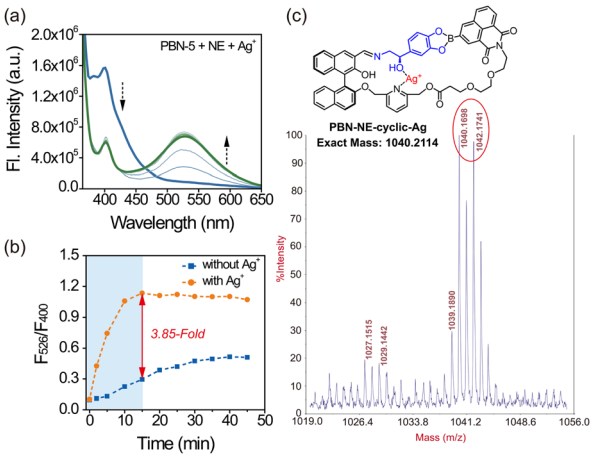

Fig. 4 The response of probe **PBN-5** towards NE in the presence of Ag^+. (a) Fluorescence spectra of **PBN-5** (10 μM) upon addition of NE (10 μM) in PBS buffer (10 mM, pH = 7.4, 10% DMSO) in the presence of Ag^+ (10 μM) for 0–50 min, excited at 350 nm. (b) Fluorescence singal at F_{526}/F_{400} of **PBN-5** upon addition of NE (10 μM) in PBS buffer (10 mM, pH = 7.4, 10% DMSO) with or without Ag^+. (c) MALDI-TOF MS of the reaction mixture of **PBN-5** with NE in the presence of Ag^+.

TOF MS of the reaction mixture exhibited a predominate signal at $m/z = 1040.2$ (Fig. 4c), indicating that one equivalent of Ag^+ was participating in the coordination.

Heteroatoms such as N/O atoms can be used as electron-donating groups to coordinate with Ag^+.[49] Multiple fluorescent probes have been reported to capture Ag^+ using N/O-containing ligands as the chelating moieties,[50,51] such as pyridine.[52–56] Considering that Ag^+ tends to form two coordination bonds, we speculated that it coordinated between the hydroxyl group of NE and the pyridyl nitrogen atom. The proposed structure of the recognition product **PBN-NE-cyclic-Ag** is illustrated in Fig. 4c, and its optimized structure was obtained by DFT calculation (B3LYP/def2TZVP), which reveals that the formation of a "silver-bridge" enhances the rigidity of the molecular system, and stabilizes the macrocyclic-ring (Fig. S11). The results suggested that Ag^+ accelerated the binding process and amplified the signal. Therefore, 1 equivalent Ag^+ was added to the system in subsequent experiments to improve the detection performance.

Quantification of NE in plasma and urine using probe PBN-5

Plasma NE is mainly released by sympathetic postganglionic neurons, serving as a sensitive indicator of SNS activity.[57–59] In contrast, urinary NE is derived from plasma NE through renal filtration, and reflects the integrated SNS activity over a period of time.[60,61] Plasma and urinary NE are both strongly associated with SNS activation: elevated levels indicate increased SNS outflow, while reduced levels may reflect sympathetic dysfunction.[16] Combined analysis of NE in plasma and urine can comprehensively evaluate the sympathetic regulation status in hypertension.[62]

Based on the high-performance of probe **PBN-5**, it was subsequently used to quantify plasma and urinary NE in SHR. To validate the efficacy of **PBN-5** in trace NE quantification, PBS buffer (pH = 8.5, 50% DMSO) was utilized as the optimal detection system. The standard curves of the **PBN-5** response to NE were obtained *via* adding different concentrations of NE and an equivalent of Ag^+. In order to achieve high-throughput detection, the emission intensity at 526 nm and 400 nm were directly recorded using a microplate reader. As a result, the linear equation was obtained ($F_{526}/F_{400} = 0.04732 \times [\mathrm{NE}]\,(\mathrm{nM}) + 0.4142$, $R^2 = 0.98$) with NE concentration in the range of 0–40 nM (Fig. S12), and the limit of detection was calculated to be 1.8 nM, demonstrating its extraordinary sensitivity to actual trace NE in plasma and urine samples.

To compare NE levels between SHR and normotensive WKY rats, blood samples and 24 hour urine (total amount of urine over a 24 hours period) samples from both groups were separately collected. Due to the matrix effects caused by complex components in plasma and urine, the samples required pretreatment to prevent interference from cells and proteins in NE detection (Fig. 5a). Thus, acetonitrile was added to precipitate proteins, followed by centrifugation to collect the supernatant, which was further lyophilized and redissolved in PBS buffer containing Ag^+. Following the addition of probe **PBN-5** to react with NE, the reaction mixture was quantified using a microplate reader. To validate the detection method, a NE standard at concentrations of 2.5, 5, 10, 15 and 20 nM was spiked into both plasma and urine samples. The recovery rates (measured NE concentration/spiked NE concentration × 100%) were calculated using **PBN-5** according to established sample pretreatment protocols and standard curve. As shown in Table S1, the measured concentration of NE showed good agreement with the spiked concentration, with the recovery rates ranged from 94.8% to 98.6% in plasma and the recovery rates ranged from 104.1% to 110.8% in urine, indicating that **PBN-5** exhibited acceptable accuracy in detecting plasma and urinary NE.

Utilizing the established method, the quantitative analysis of NE was performed in blood and urine samples from SHR and control WKY rats. The signal of F_{526}/F_{400} was significantly higher in both plasma (1.43-fold) and urine (1.38-fold) of SHR compared to WKY rats (Fig. 5b and c). The quantitative analysis results demonstrated that the plasma NE in WKY rats ranged from 4.24 nM to 15.36 nM, while the value measured in SHR ranged from 6.21 nM to 31.51 nM. Meanwhile, the urinary NE in WKY rats ranged from 6.76 nM to 8.68 nM, while the value measured in SHR ranged from 11.54 nM to 16.02 nM (Fig. 5d). The above results suggested that SHR have higher NE levels in plasma and urine, which indicated the SNS overactivation in spontaneous hypertension.

Fluorescence imaging of NE in living cells and tissues using probe PBN-5

The desirable characteristics of **PBN-5** *in vitro* imply its potential for NE imaging in biological systems. To assess its biosafety, the cytotoxicity of the probe was evaluated using CCK-8 assay. As shown in Fig. S13, treatment with **PBN-5** at varying concentrations (2, 4, 8, 10, 15, and 20 μM) for 24 h maintained cell viability above 80% in HepG2 (human hepatocellular carcinoma), 4T1 (mouse mammary carcinoma) and PC12 (rat

© 2025 The Author(s). Published by the Royal Society of Chemistry

Open Access Article. Published on 15 September 2025. Downloaded on 2/10/2026 10:16:37 AM. This article is licensed under a Creative Commons Attribution-NonCommercial 3.0 Unported Licence.

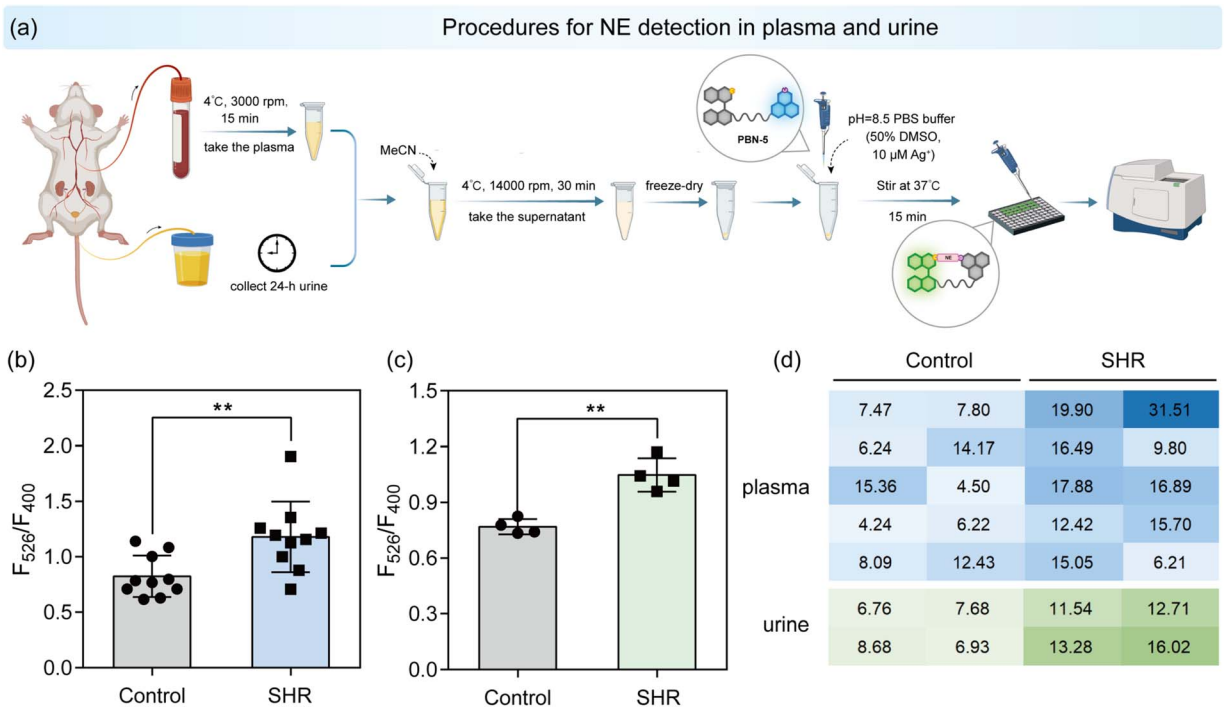

Fig. 5 Quantitative detection of NE in plasma and urine from SHR and WKY rats using probe **PBN-5**. (a) Schematic diagram of sample pretreatment and NE quantification in rat plasma/urine using the probe **PBN-5**. (b) The fluorescence signals at F_{526}/F_{400} obtained from NE detection in plasma of SHR and WKY rats using probe **PBN-5**. Data are presented as mean ± S.D. Error bars: S.D., $n = 10$ independent rats samples, black dots represent individual data points. Statistical significance is calculated with a two-tailed unpaired *t* test (**$p < 0.01$). (c) The fluorescence signals at F_{526}/F_{400} obtained from NE detection in urine of SHR and WKY rats using probe **PBN-5**. Data are presented as mean ± S.D. Error bars: S.D., $n = 4$ independent rats samples, black dots represent individual data points. Statistical significance is calculated with a two-tailed unpaired *t* test (**$p < 0.01$). (d) The heatmap analysis of quantitative NE concentrations in plasma and urine between SHR and WKY rats.

adrenal medulla pheochromocytoma) cells, confirming its low cytotoxicity and excellent biocompatibility.

It has been reported that PC12 cells can synthesize and secrete NE.[63] Therefore, the incubation time was systematically optimized by treating PC12 cells with **PBN-5** for varying durations (0, 15, 30, 60, 90, 120, 180 and 240 min). As shown in Fig. S14, the fluorescence intensity was observed to increase progressively over time until reaching a plateau at 60 min, establishing this incubation time as optimal for subsequent experiments. The capability of **PBN-5** for visualizing endogenous NE was subsequently explored in different cells. **PBN-5** was incubated with HepG2, 4T1 and PC12 cells for 60 min, and then the fluorescence imaging was performed. As shown in Fig. 6a and b, only PC12 cells exhibited obvious green fluorescence, and basically no emission intensity was observed in HepG2 and 4T1 cells. These results confirmed that PC12 cells contain a large amount of NE, which can be effectively visualized by probe **PBN-5**.

Moreover, NE is primarily released from neuronal cells *via* exocytosis and acts on adrenergic receptors. Thus, the probe was further used to monitor the secretion process of NE stimulated by high-K^+ solution (a mimic of electrical impulse). Upon high concentration K^+ (1 mM) stimulation, a rapid decrease in fluorescence intensity was observed within 30 s (to 48.7% of the initial intensity), which may be due to the decrease of intracellular NE levels attributed to K^+-induced exocytosis (Fig. S15). In contrast, when stimulated with PBS (without K^+), negligible change in green channel fluorescence was observed. These results demonstrated that **PBN-5** can reflect the endogenous NE changes and visualize the exocytosis process in living PC12 cells. Subsequently, PC12 cells pretreated with varying NE concentrations (0, 0.1, 0.5, 1 mM) were incubated with the probe for 60 min. As shown in Fig. 6c and d, the fluorescence intensity in cells increased proportionally with intracellular NE levels. The results further confirmed that probe **PBN-5** can effectively monitor the change of intracellular NE levels.

Based on the performance of **PBN-5** for NE visualization at the cellular level, we further applied the probe to tissue imaging of SHR and normotensive WKY rats. Sympathetic nerve enriched tissues (heart, kidney and adrenal medulla) were processed for fluorescence imaging. As shown in Fig. 6e and f, the fluorescence intensity in heart and kidney tissues of SHR was much higher than that of control group. We further performed the staining analysis of rat adrenal glands. H&E staining enables differentiation of the adrenal medulla from the outer cortex based on the distinct morphological characteristics (Fig. 6g). Then, the average fluorescence intensity of the medulla outlined by the white dashed line was calculated using H&E-stained images as a reference. Stronger fluorescence was observed in adrenal medulla than cortex in both SHR and normotensive WKY rats. These results indicated that NE is distributed in the medulla region, which was supported by the

Open Access Article. Published on 15 September 2025. Downloaded on 2/10/2026 10:16:37 AM.
This article is licensed under a Creative Commons Attribution-NonCommercial 3.0 Unported Licence.

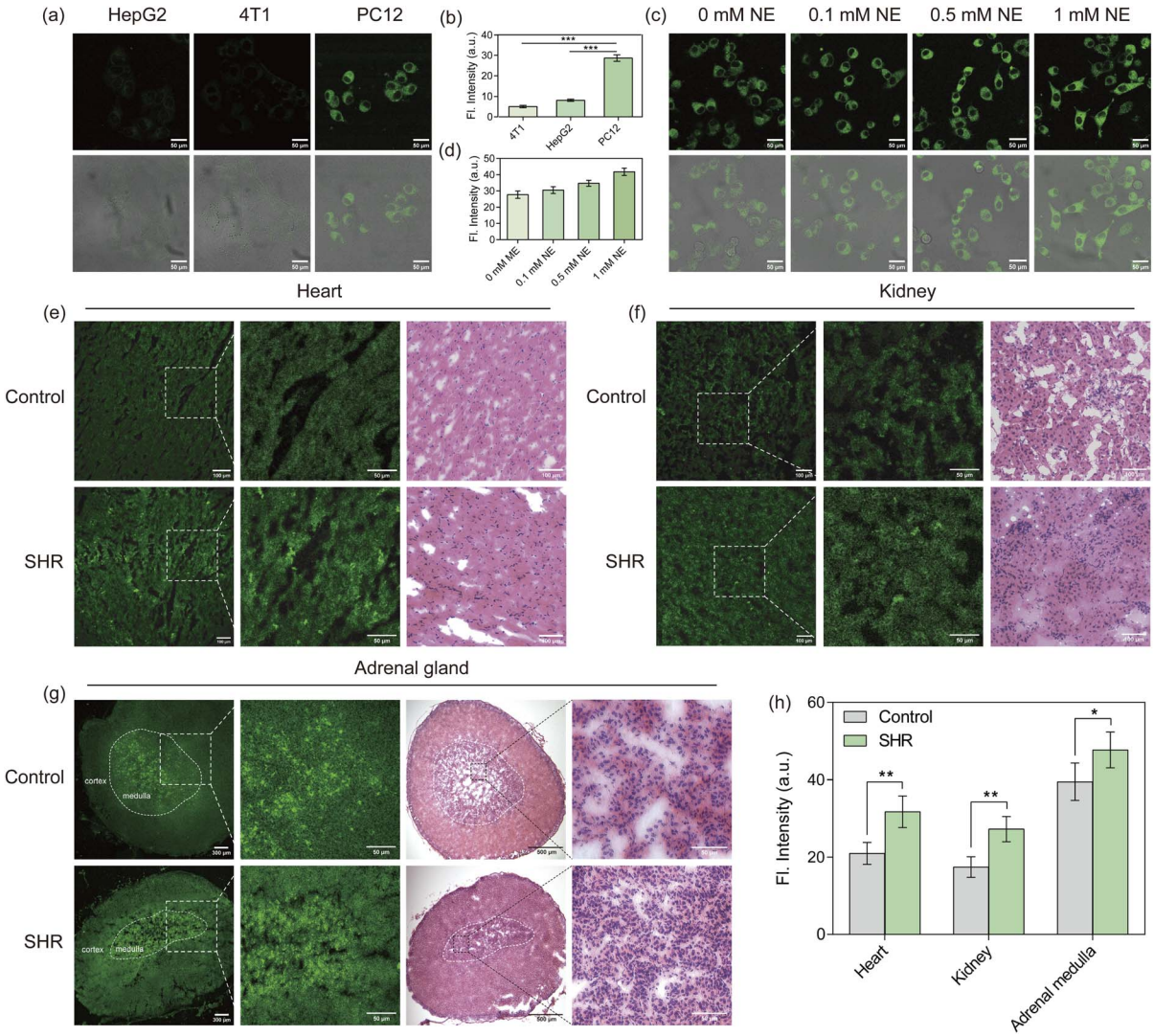

Fig. 6 Confocal imaging for NE in cells and tissues using probe **PBN-5**. (a) Confocal imaging for endogenous NE in HepG2 cells, 4T1 cells and PC12 cells treated with **PBN-5** (10 μM), excited at 405 nm. (b) Quantitative analysis of the fluorescence intensity in HepG2 cells, 4T1 cells and PC12 cells. Data are presented as mean ± S.D. Error bars: S.D., $n = 3$ independent experiments. Statistical significance is calculated with a two-tailed unpaired t test (***$p < 0.001$). (c) Confocal imaging of NE at varying concentrations (0 mM, 0.1 mM, 0.5 mM, 1 mM) using **PBN-5** in PC12 cells. (d) Quantitative analysis of fluorescence intensity of the probe in response to varying NE concentrations. Data are presented as mean ± S.D. Error bars: S.D., $n = 3$ independent experiments. (e–g) Comparative confocal imaging of NE and H&E staining in heart (e), kidney (f) and adrenal gland (g) tissues of SHR and control WKY rats, excited at 405 nm. (h) Quantitative analysis of the fluorescence intensity in heart, kidney and adrenal medulla of SHR and control WKY rats. Data are presented as mean ± S.D. Error bars: S.D., $n = 3$ rats. Statistical significance is calculated with a two-tailed unpaired t test (*$p < 0.05$, **$p < 0.01$).

reported mass spectrometry imaging of adrenal NE.[64] Notably, the adrenal medulla of SHR exhibited slightly stronger fluorescence signals compared to the control group, suggesting marginally elevated NE concentration in adrenal gland of SHR (Fig. 6g and h). These results provided direct evidence for elevated tissue NE levels in hypertension. Combined with quantitative measurements of plasma and urinary NE, these findings demonstrated the activation of the sympathetic-adrenal axis in hypertension. The elevated NE may contribute to the blood pressure by activating α1/β1 receptors. As such, this study could provide key insights into the progression assessment and disease mechanisms of hypertension.

Conclusion

In summary, we have designed and synthesized a dual-site ratiometric fluorescent probe **PBN-5** for precisely quantifying trace NE based on a macrocyclic recognition strategy. To specifically recognize the unique L-hydroxyethylamine and catechol moieties of NE, an aldehyde-substituted chiral binaphthyl and boronic acid groups were introduced to probe **PBN-5**. The detection process is based on a nucleophilic reaction between the aldehyde and amino group, and a condensation reaction between the boronic acid group and catechol, forming a macrocyclic-ring enhanced by silver bridging. By

© 2025 The Author(s). Published by the Royal Society of Chemistry

Open Access Article. Published on 15 September 2025. Downloaded on 2/10/2026 10:16:37 AM. This article is licensed under a Creative Commons Attribution-NonCommercial 3.0 Unported Licence.

utilizing the probe **PBN-5** for both NE quantification in plasma/urine and fluorescence imaging in tissue sections, we demonstrated the elevated circulating and tissue NE levels in spontaneous hypertension, indicating sympathetic nervous overexcitation. This study establishes a novel chemical approach for NE recognition, providing a molecular tool to deepen the understanding of NE levels and sympathetic activity in spontaneous hypertension. Future efforts will focus on applying the probe to clinical human samples, with particular attention to the more complex matrices compared to rodent models, as well as simplifying the pretreatment procedures. Meanwhile, a better matching of the reaction kinetics and binding constants between the two recognition sites is expected to further enhance the detection performance of the probe, while red-shifted wavelength is also crucial for improving the signal-to-noise ratio for *in vivo* imaging applications.

Author contributions

F. Wang carried out the experiments, analyzed the data, and wrote the original manuscript. J. Wang analyzed the data and participated in the discussion. W. Zhu and Y. Yang guided writing and edited the manuscript. Y. Xu, H. Li supervised the whole project & guided writing, reviewed, and edited the manuscript. T. D. James guided writing, reviewed, and edited the manuscript.

Conflicts of interest

There are no conflicts to declare.

Data availability

Reasonable requests for additional information can be made to the corresponding authors. The animal experiments were conducted under the protocol approved by the Scientific Investigation Board of East China University of Science and Technology (ECUST-2025-148).

The data supporting this article have been included as part of the SI. A detailed experimental methods, synthesis, structural characterizations, $^{1}H/^{13}C$ NMR, HRMS spectra and additional experimental data supporting this article have been provided in the SI. See DOI: **https://doi.org/10.1039/d5sc05925a**.

Acknowledgements

This work is financially supported by National Key Research and Development Programs (2022YFD1700403 and 2023YFD1700303). The authors wish to thank Prof. Amilra Prasanna de Silva, for his valuable and thoughtful suggestions on this paper. TDJ wishes to thank the University of Bath and the Open Research Fund of the School of Chemistry and Chemical Engineering, Henan Normal University (2020ZD01) for support.

References

1 G. Parati and M. Esler, The human sympathetic nervous system: its relevance in hypertension and heart failure, *Eur. Heart J.*, 2012, **33**, 1058–1066.
2 G. F. DiBona, Sympathetic Nervous System and Hypertension, *Hypertension*, 2013, **61**, 556–560.
3 B. J. Matchett, L. T. Grinberg, P. Theofilas and M. E. Murray, The mechanistic link between selective vulnerability of the locus coeruleus and neurodegeneration in Alzheimer's disease, *Acta Neuropathol.*, 2021, **141**, 631–650.
4 M. E. Fox and R. M. Wightman, Contrasting Regulation of Catecholamine Neurotransmission in the Behaving Brain: Pharmacological Insights from an Electrochemical Perspective, *Pharmacol. Rev.*, 2017, **69**, 12–32.
5 D. G. Bernabé, Catecholamines Mediate Psychologic Stress-Induced Cancer Progression, *Cancer Res.*, 2021, **81**, 5144–5146.
6 K. B. Lefton, Y. Wu, Y. Dai, T. Okuda, Y. Zhang, A. Yen, G. M. Rurak, S. Walsh, R. Manno, B.-E. Myagmar, J. D. Dougherty, V. K. Samineni, P. C. Simpson and T. Papouin, Norepinephrine signals through astrocytes to modulate synapses, *Science*, 2025, **388**, 776–783.
7 J. Ng, A. Papandreou, S. J. Heales and M. A. Kurian, Monoamine neurotransmitter disorders-clinical advances and future perspectives, *Nat. Rev. Neurol.*, 2015, **11**, 567–584.
8 G. Eisenhofer, I. J. Kopin and D. S. Goldstein, Catecholamine Metabolism: A Contemporary View with Implications for Physiology and Medicine, *Pharmacol. Rev.*, 2004, **56**, 331–349.
9 J. L. Hall, T. D. O'Connell and G. S. Francis, Promising Small Molecule for Heart Failure Targeting Adrenal Catecholamine Release and β-Adrenergic Receptor Signaling in the Heart, *J. Am. Coll. Cardiol.*, 2014, **63**, 2558–2559.
10 W. Bougouin, K. Slimani, M. Renaudier, Y. Binois, M. Paul, F. Dumas, L. Lamhaut, T. Loeb, S. Ortuno, N. Deye, S. Voicu, F. Beganton, D. Jost, A. Mekontso-Dessap, E. Marijon, X. Jouven, N. Aissaoui and A. Cariou, Epinephrine *versus* norepinephrine in cardiac arrest patients with post-resuscitation shock, *Intensive Care Med.*, 2022, **48**, 300–310.
11 J. Myburgh, Norepinephrine: more of a neurohormone than a vasopressor, *Crit. Care*, 2010, **14**, 196.
12 V. Breton-Provencher, G. T. Drummond, J. Feng, Y. Li and M. Sur, Spatiotemporal dynamics of noradrenaline during learned behaviour, *Nature*, 2022, **606**, 732–738.
13 D. T. Andreis and M. Singer, Catecholamines for inflammatory shock: a Jekyll-and-Hyde conundrum, *Intensive Care Med.*, 2016, **42**, 1387–1397.
14 A. M. Wengrowski, X. Wang, S. Tapa, N. G. Posnack, D. Mendelowitz and M. W. Kay, Optogenetic release of norepinephrine from cardiac sympathetic neurons alters mechanical and electrical function, *Cardiovasc. Res.*, 2015, **105**, 143–150.
15 B. Zhang, S. Ma, I. Rachmin, M. He, P. Baral, S. Choi, W. A. Gonçalves, Y. Shwartz, E. M. Fast, Y. Su, L. I. Zon, A. Regev, J. D. Buenrostro, T. M. Cunha, I. M. Chiu,

Open Access Article. Published on 15 September 2025. Downloaded on 2/10/2026 10:16:37 AM. This article is licensed under a Creative Commons Attribution-NonCommercial 3.0 Unported Licence.

D. E. Fisher and Y.-C. Hsu, Hyperactivation of sympathetic nerves drives depletion of melanocyte stem cells, *Nature*, 2020, **577**, 676–681.

16 G. Grassi, A. Mark and M. Esler, The Sympathetic Nervous System Alterations in Human Hypertension, *Circ. Res.*, 2015, **116**, 976–990.

17 D. Carnevale and G. Lembo, Heart, Spleen, Brain, *Circulation*, 2018, **138**, 1917–1919.

18 C. Ye, F. Zheng, T. Xu, N. Wu, Y. Tong, X.-Q. Xiong, Y.-B. Zhou, J.-J. Wang, Q. Chen, Y.-H. Li, G.-Q. Zhu and Y. Han, Norepinephrine acting on adventitial fibroblasts stimulates vascular smooth muscle cell proliferation *via* promoting small extracellular vesicle release, *Theranostics*, 2022, **12**, 4718–4733.

19 P. H. Wirtz, U. Ehlert, C. Bärtschi, L. S. Redwine and R. von Känel, Changes in plasma lipids with psychosocial stress are related to hypertension status and the norepinephrine stress response, *Metabolism*, 2009, **58**, 30–37.

20 J. T. Davis, F. Rao, D. Naqshbandi, M. M. Fung, K. Zhang, A. J. Schork, C. M. Nievergelt, M. G. Ziegler and D. T. O'Connor, Autonomic and Hemodynamic Origins of Pre-Hypertension: Central Role of Heredity, *J. Am. Coll. Cardiol.*, 2012, **59**, 2206–2216.

21 T. Kanamori, T. Funatsu and M. Tsunoda, Determination of catecholamines and related compounds in mouse urine using column-switching HPLC, *Analyst*, 2016, **141**, 2568–2573.

22 L. Chen, Y. Bi, T. Xu, X. Li and Z. Fang, Composite Nanofibers as Novel Sorbents for On-Line and Off-Line Solid-Phase Extraction in Chromatographic System: A Comparison for Detection of Free Biogenic Monoamines and Their Metabolites in Plasma, *Molecules*, 2022, **27**, 6971.

23 J. A. Ribeiro, P. M. V. Fernandes, C. M. Pereira and F. Silva, Electrochemical sensors and biosensors for determination of catecholamine neurotransmitters: a review, *Talanta*, 2016, **160**, 653–679.

24 S. Boobphahom, T. Siripongpreda, D. Zhang, J. Qin, P. Rattanawaleedirojn and N. Rodthongkum, TiO_2/MXene-PVA/GO hydrogel-based electrochemical sensor for neurological disorder screening *via* urinary norepinephrine detection, *Microchim. Acta*, 2021, **188**, 387.

25 R. N. Goyal, M. A. Aziz, M. Oyama, S. Chatterjee and A. R. S. Rana, Nanogold based electrochemical sensor for determination of norepinephrine in biological fluids, *Sens. Actuators, B*, 2011, **153**, 232–238.

26 S. Gu, D. Xu, J. Huang, X. Zhou, Y. Liu and Z. Zhang, Photoelectrochemical biosensor with single atom sites for norepinephrine sensing and brain region synergy in epilepsy, *Nat. Commun.*, 2025, **16**, 4765.

27 L. Mao, Y. Han, Q.-W. Zhang and Y. Tian, Two-photon fluorescence imaging and specifically biosensing of norepinephrine on a 100-ms timescale, *Nat. Commun.*, 2023, **14**, 1419.

28 Y. Han, L. Mao, Q.-W. Zhang and Y. Tian, Sub-100 ms Level Ultrafast Detection and Near-Infrared Ratiometric Fluorescence Imaging of Norepinephrine in Live Neurons and Brains, *J. Am. Chem. Soc.*, 2023, **145**, 23832–23841.

29 H. Yan, Y. Wang, F. Huo and C. Yin, Fast-Specific Fluorescent Probes to Visualize Norepinephrine Signaling Pathways and Its Flux in the Epileptic Mice Brain, *J. Am. Chem. Soc.*, 2023, **145**, 3229–3237.

30 N. Zhou, F. Huo, Y. Yue and C. Yin, Specific Fluorescent Probe Based on "Protect-Deprotect" To Visualize the Norepinephrine Signaling Pathway and Drug Intervention Tracers, *J. Am. Chem. Soc.*, 2020, **142**, 17751–17755.

31 Y. Zhao, Y. Mei, J. Sun and Y. Tian, A Supramolecular Fluorescent Chemosensor Enabling Specific and Rapid Quantification of Norepinephrine Dynamics, *J. Am. Chem. Soc.*, 2025, **147**, 5025–5034.

32 K. E. Secor and T. E. Glass, Selective Amine Recognition: Development of a Chemosensor for Dopamine and Norepinephrine, *Org. Lett.*, 2004, **6**, 3727–3730.

33 L. Zhang, X. A. Liu, K. D. Gillis and T. E. Glass, Synthesis of a Near-Infrared Fluorescent Probe for Imaging Catecholamines *via* a Tandem Nucleophilic Aromatic Substitution, *Org. Lett.*, 2023, **25**, 9103–9107.

34 L. Zhang, X. A. Liu, K. D. Gillis and T. E. Glass, A High-Affinity Fluorescent Sensor for Catecholamine: Application to Monitoring Norepinephrine Exocytosis, *Angew. Chem., Int. Ed.*, 2019, **58**, 7611–7614.

35 A. Bade, P. Yadav, L. Zhang, R. Naidu Bypaneni, M. Xu and T. E. Glass, Imaging Neurotransmitters with Small-Molecule Fluorescent Probes, *Angew. Chem., Int. Ed.*, 2024, **63**, e202406401.

36 K. S. Hettie, X. Liu, K. D. Gillis and T. E. Glass, Selective Catecholamine Recognition with NeuroSensor 521: A Fluorescent Sensor for the Visualization of Norepinephrine in Fixed and Live Cells, *ACS Chem. Neurosci.*, 2013, **4**, 918–923.

37 J. Krämer, R. Kang, L. M. Grimm, L. De Cola, P. Picchetti and F. Biedermann, Molecular Probes, Chemosensors, and Nanosensors for Optical Detection of Biorelevant Molecules and Ions in Aqueous Media and Biofluids, *Chem. Rev.*, 2022, **122**, 3459–3636.

38 M. H. Lee, J. S. Kim and J. L. Sessler, Small molecule-based ratiometric fluorescence probes for cations, anions, and biomolecules, *Chem. Soc. Rev.*, 2015, **44**, 4185–4191.

39 R. Gui, H. Jin, X. Bu, Y. Fu, Z. Wang and Q. Liu, Recent advances in dual-emission ratiometric fluorescence probes for chemo/biosensing and bioimaging of biomarkers, *Coord. Chem. Rev.*, 2019, **383**, 82–103.

40 M. R. Smith, L. Zhang, Y. Jin, M. Yang, A. Bade, K. D. Gillis, S. Jana, R. N. Bypaneni, T. E. Glass and H. Lin, A Turn-On Fluorescent Amino Acid Sensor Reveals Chloroquine's Effect on Cellular Amino Acids *via* Inhibiting Cathepsin L, *ACS Cent. Sci.*, 2023, **9**, 980–991.

41 Y. Mao, S. Davis and L. Pu, Regio- and Enantioselective Macrocyclization from Dynamic Imine Formation: Chemo- and Enantioselective Fluorescent Recognition of Lysine, *Org. Lett.*, 2023, **25**, 7639–7644.

42 J. Tian, S. Yu, H. Guo, M. Zhu, K. Lu, Y. Jiang, J. Yang, X. Yu and L. Pu, Enantioselective Fluorescent Recognition of β-Amino Alcohols by Stereoselective Cyclization, *Eur. J. Org Chem.*, 2022, **2022**, e202200283.

© 2025 The Author(s). Published by the Royal Society of Chemistry

Open Access Article. Published on 15 September 2025. Downloaded on 2/10/2026 10:16:37 AM. This article is licensed under a Creative Commons Attribution-NonCommercial 3.0 Unported Licence.

43 G. Sun, X. Zhang, Z. Zheng, Z.-Y. Zhang, M. Dong, J. L. Sessler and C. Li, Chiral Macrocycles for Enantioselective Recognition, *J. Am. Chem. Soc.*, 2024, **146**, 26233–26242.

44 Y. Mao, M. A. Abed, N. B. Lee, X. Wu, G. Du and L. Pu, Determining the concentration and enantiomeric composition of histidine using one fluorescent probe, *Chem. Commun.*, 2021, **57**, 587–590.

45 L. Pu, Enantioselective Fluorescent Recognition of Free Amino Acids: Challenges and Opportunities, *Angew. Chem., Int. Ed.*, 2020, **59**, 21814–21828.

46 Y.-Y. Zhu, X.-D. Wu, S.-X. Gu and L. Pu, Free Amino Acid Recognition: A Bisbinaphthyl-Based Fluorescent Probe with High Enantioselectivity, *J. Am. Chem. Soc.*, 2019, **141**, 175–181.

47 Y. Mao, E. Thomae, S. Davis, C. Wang, Y. Li and L. Pu, One Molecular Probe with Opposite Enantioselective Fluorescence Enhancement at Two Distinct Emissions, *Org. Lett.*, 2023, **25**, 2157–2161.

48 Z. Huang, S. Yu, K. Wen, X. Yu and L. Pu, Zn(II) promoted dramatic enhancement in the enantioselective fluorescent recognition of functional chiral amines by a chiral aldehyde, *Chem. Sci.*, 2014, **5**, 3457–3462.

49 M. She, Z. Wang, J. Chen, Q. Li, P. Liu, F. Chen, S. Zhang and J. Li, Design strategy and recent progress of fluorescent probe for noble metal ions (Ag, Au, Pd, and Pt), *Coord. Chem. Rev.*, 2021, **432**, 213712.

50 H. Wu, J. Jia, Y. Xu, X. Qian and W. Zhu, A reusable bifunctional fluorescent sensor for the detection and removal of silver ions in aqueous solutions, *Sens. Actuators, B*, 2018, **265**, 59–66.

51 J. Kang, M. Choi, J. Y. Kwon, E. Y. Lee and J. Yoon, New Fluorescent Chemosensors for Silver Ion, *J. Org. Chem.*, 2002, **67**, 4384–4386.

52 S. S. Chunikhin, I. N. Bardasov, R. A. Akasov and O. V. Ershov, New "turn-on" chemosensor for fluorescence detection of silver (I) based on tetracyanopyridine (TCPy), *Dyes Pigm.*, 2022, **205**, 110516.

53 K. Li, T. Liu, J. Ying, A. Tian and X. Wang, A POM/viologen-based supramolecular fluorescent probe for Ag^+ detection and application of visible hydrogel based intelligent sensing system, *Dyes Pigm.*, 2024, **222**, 111898.

54 M. Sahu, A. Kumar Manna, K. Rout, J. Mondal and G. K. Patra, A highly selective thiosemicarbazone based Schiff base chemosensor for colorimetric detection of Cu^{2+} and Ag^+ ions and turn-on fluorometric detection of Ag^+ ions, *Inorg. Chim. Acta*, 2020, **508**, 119633.

55 J.-H. Ye, L. Duan, C. Yan, W. Zhang and W. He, A new ratiometric Ag^+ fluorescent sensor based on aggregation-induced emission, *Tetrahedron Lett.*, 2012, **53**, 593–596.

56 Y. Zhang, D. Wang, C. Sun, H. Feng, D. Zhao and Y. Bi, A simple 2,6-diphenylpyridine-based fluorescence "turn-on" chemosensor for Ag^+ with a high luminescence quantum yield, *Dyes Pigm.*, 2017, **141**, 202–208.

57 D. S. Goldstein, Plasma catecholamines and essential hypertension. An analytical review, *Hypertension*, 1983, **5**, 86–99.

58 G. Grassi and M. Esler, How to assess sympathetic activity in humans, *J. Hypertens.*, 1999, **17**, 719–734.

59 G. Grassi, A. Pisano, D. Bolignano, G. Seravalle, G. D'Arrigo, F. Quarti-Trevano, F. Mallamaci, C. Zoccali and G. Mancia, Sympathetic Nerve Traffic Activation in Essential Hypertension and Its Correlates, *Hypertension*, 2018, **72**, 483–491.

60 F. Saladini, L. Mos, C. Fania, A. Mazzer, G. Garavelli, G. Zanata, P. Spinella and P. Palatini, Gender related differences in the clinical significance of elevated pulse pressure in the young. Results from the HARVEST study, *Eur. Heart J.*, 2019, **40**, 3349.

61 D. Robertson, G. A. Johnson, R. M. Robertson, A. S. Nies, D. G. Shand and J. A. Oates, Comparative assessment of stimuli that release neuronal and adrenomedullary catecholamines in man, *Circulation*, 1979, **59**, 637–643.

62 G. Grassi, Assessment of Sympathetic Cardiovascular Drive in Human Hypertension, *Hypertension*, 2009, **54**, 690–697.

63 R. H. S. Westerink and A. G. Ewing, The PC12 cell as model for neurosecretion, *Acta Physiol.*, 2008, **192**, 273–285.

64 I. Kaya, S. M. Brülls, J. Dunevall, E. Jennische, S. Lange, J. Mårtensson, A. G. Ewing, P. Malmberg and J. S. Fletcher, On-Tissue Chemical Derivatization of Catecholamines Using 4-(*N*-Methyl)pyridinium Boronic Acid for ToF-SIMS and LDI-ToF Mass Spectrometry Imaging, *Anal. Chem.*, 2018, **90**, 13580–13590.

© 2025 The Author(s). Published by the Royal Society of Chemistry